



AFRL-RZ-WP-TP-2012-0158

**TRAJECTORY, DEVELOPMENT, AND TEMPERATURE OF
SPARK KERNELS EXITING INTO QUIESCENT AIR
(PREPRINT)**

Barry V. Kiel

**Propulsion Branch
Turbine Engine Division**

David Blunck

Purdue University

APRIL 2012

Approved for public release; distribution unlimited.

See additional restrictions described on inside pages

STINFO COPY

**AIR FORCE RESEARCH LABORATORY
PROPULSION DIRECTORATE
WRIGHT-PATTERSON AIR FORCE BASE, OH 45433-7251
AIR FORCE MATERIEL COMMAND
UNITED STATES AIR FORCE**

REPORT DOCUMENTATION PAGE				<i>Form Approved</i> OMB No. 0704-0188	
The public reporting burden for this collection of information is estimated to average 1 hour per response, including the time for reviewing instructions, searching existing data sources, gathering and maintaining the data needed, and completing and reviewing the collection of information. Send comments regarding this burden estimate or any other aspect of this collection of information, including suggestions for reducing this burden, to Department of Defense, Washington Headquarters Services, Directorate for Information Operations and Reports (0704-0188), 1215 Jefferson Davis Highway, Suite 1204, Arlington, VA 22202-4302. Respondents should be aware that notwithstanding any other provision of law, no person shall be subject to any penalty for failing to comply with a collection of information if it does not display a currently valid OMB control number. PLEASE DO NOT RETURN YOUR FORM TO THE ABOVE ADDRESS.					
1. REPORT DATE (DD-MM-YY) April 2012		2. REPORT TYPE Technical Paper Preprint		3. DATES COVERED (From - To) 01 April 2010 – 01 April 2012	
4. TITLE AND SUBTITLE TRAJECTORY, DEVELOPMENT, AND TEMPERATURE OF SPARK KERNELS EXITING INTO QUIESCENT AIR (PREPRINT)				5a. CONTRACT NUMBER In-house	
				5b. GRANT NUMBER	
				5c. PROGRAM ELEMENT NUMBER 62203F	
6. AUTHOR(S) Barry V. Kiel (AFRL/RZTP) David Blunck (Purdue University)				5d. PROJECT NUMBER 3066	
				5e. TASK NUMBER 05	
				5f. WORK UNIT NUMBER 306605AR	
7. PERFORMING ORGANIZATION NAME(S) AND ADDRESS(ES) Propulsion Branch (AFRL/RZTP) Turbine Engine Division Air Force Research Laboratory, Propulsion Directorate Wright-Patterson Air Force Base, OH 45433-7251 Air Force Materiel Command, United States Air Force				8. PERFORMING ORGANIZATION REPORT NUMBER AFRL-RZ-WP-TP-2012-0158	
9. SPONSORING/MONITORING AGENCY NAME(S) AND ADDRESS(ES) Air Force Research Laboratory Propulsion Directorate Wright-Patterson Air Force Base, OH 45433-7251 Air Force Materiel Command United States Air Force				10. SPONSORING/MONITORING AGENCY ACRONYM(S) AFRL/RZTP	
				11. SPONSORING/MONITORING AGENCY REPORT NUMBER(S) AFRL-RZ-WP-TP-2012-0158	
12. DISTRIBUTION/AVAILABILITY STATEMENT Approved for public release; distribution unlimited.					
13. SUPPLEMENTARY NOTES Paper contains color. PA Case Number: 88ABW-2010-3621; Clearance Date: 30 Jun 2010.					
14. ABSTRACT An inverse deconvolution technique was developed to determine the temperature and sensible energy of the kernels. This technique is evaluated by a sensitivity analysis and comparisons to measurements on a well characterized flame. Infrared images show that the kernels develop into a toroidal shape after exiting from the igniter. The statistical distribution of the trajectory of spark kernels is symmetric. Buoyancy forces have a negligible effect on the trajectory. Regions of high and low radiation intensity are observed in the kernels, indicating temperature gradients within the gases. The radiation intensity emitted by spark kernels decreases by more than an order of magnitude after exiting the igniter. Average temperature values decrease by less than 30% over 2 cm of the spark trajectory. Over that distance the sensible energy of the kernel decreases by 80%.					
15. SUBJECT TERMS augmentor, dynamic stability, screech, flame holder, gas-turbine propulsion, combustion					
16. SECURITY CLASSIFICATION OF:			17. LIMITATION OF ABSTRACT: SAR	18. NUMBER OF PAGES 18	19a. NAME OF RESPONSIBLE PERSON (Monitor) Barry V. Kiel 19b. TELEPHONE NUMBER (Include Area Code) N/A
a. REPORT Unclassified	b. ABSTRACT Unclassified	c. THIS PAGE Unclassified			

Trajectory, Development, and Temperature of Spark Kernels Exiting into Quiescent Air

David L. Blunck¹

Purdue University, West Lafayette, IN, 47907

Barry V. Kiel²

Air Force Research Laboratory, Dayton, OH, 45433

Measurements of the trajectory, spatial development, and temperature of spark kernels are needed for understanding the ignition process in spark ignition and gas turbine engines. Motivated by this, an infrared camera was used to obtain spectrally and path integrated radiation intensity measurements of spark kernels exiting into quiescent air. An inverse deconvolution technique was developed to determine the temperature and sensible energy of the kernels. This technique is evaluated by a sensitivity analysis and comparisons to measurements on a well characterized flame. Infrared images show that the kernels develop into a toroidal shape after exiting from the igniter. The statistical distribution of the trajectory of spark kernels is symmetric. Buoyancy forces have a negligible effect on the trajectory. Regions of high and low radiation intensity are observed in the kernels, indicating temperature gradients within the gases. The radiation intensity emitted by spark kernels decreases by more than an order of magnitude after exiting the igniter. Average temperature values decrease by less than 30% over 2 cm of the spark trajectory. Over that distance the sensible energy of the kernel decreases by 80%.

I. Introduction

Infrared radiation intensity measurements were obtained of spark kernels exiting from a pulsed plasma jet igniter into quiescent air. These measurements provide qualitative insights into the development of spark kernels and quantitative values for the temperature and sensible energy of the heated gases. The motivation for this work is twofold. First, lean combustion in spark ignition and gas turbine engines is desirable for improved efficiency and decreased pollutant formation¹⁻⁶. Lean fuel conditions, however, can be more difficult to consistently ignite⁷. Measurements of the spatial and temporal development of the temperature field within the kernel are needed for understanding the ignition process near flammability limits. The second motivation for this work is to obtain scalar data of spark kernels which can be used for validating numerical models. Ekici et al.¹ noted that limited scalar data is available.

In its simplest description, a spark is an electrical discharge in which a portion of the energy is transferred to plasma and the surrounding fluid and the remaining portion is lost to the electrodes. The spark event is often classified as the prebreakdown, breakdown, arc, and glow phases. The former three phases cumulatively last on the order of microseconds, while the glow phase can last on the order of milliseconds⁴. Standard ignition systems typically deliver 30 to 50 mJ of energy to the spark⁸. Measurements of the energy delivered by sparks typically have been obtained by measuring pressure changes in a calorimeter⁹⁻¹².

Ignition of a flammable mixture occurs when the chemical reactions become self sustaining, typically some time after the spark event. Zhang et al. reported that several milliseconds elapsed between when the spark kernel was no longer luminous and when combustion was detected¹³. Naegeli and Dodge noted that visible radiation from a flame kernel was detected 8 to 13 milliseconds after the spark in a gas turbine combustor⁵. Maly noted that CN radicals are evident soon after the spark (order of nanoseconds), but OH and CO molecules occur about 10 milliseconds after the spark⁷.

¹ Graduate Research Assistant, School of Mechanical Engineering, 500 Allison Road, AIAA Member

² Senior Mechanical Engineer, Combustion Branch, Air Force Research Laboratory, and Senior AIAA Member.

The kernel which results from the spark expands and mixes with the surrounding gases^{14,15}. Both the temperature and size of the kernel affect whether ignition occurs. Temperature measurements reported for spark kernels typically have been found using interferogram measurements of a known light source^{9,16,17}, although these have been limited. Reinmann and Akram reported temperature values of 30,000 and 23,000 K, 1 and 5 microseconds (respectively) after the spark⁹. Topham et al. reported that the temperature of kernels exiting from a pulsed plasma igniter with a stored energy of 4.8 J were 400 to 20 K above the ambient temperature 0.2 to 7 milliseconds (respectively) after the spark. The temperatures decreased to values of 40 to 10 K above ambient 2 to 9 ms after the spark when 0.98 J was delivered to the igniter¹⁶. Laser-schlieren visualization and Rayleigh laser light scattering have been used to determine the size and development of spark kernels^{2,13,14-16}. The critical spark radius (i.e. the maximum detectable radius which the kernel will expand without ignition) is typically on the order of 0.5 cm¹².

Given the importance of understanding the temporal and spatial development of a spark and the limited scalar data which is available, the objectives of this work are as follows:

- 1) Obtain infrared images of the temporal and spatial development of spark kernels.
- 2) Measure the magnitude and decay of the radiation intensity emitted by the kernel gases.
- 3) Determine the mean temperature within the kernel.
- 4) Determine the sensible energy of the kernel gases.

II. Experimental Approach

A. Spark Generation

Spark kernels were generated using a pulsed plasma jet igniter. This type of igniter has received considerable interest,^{10,11,16,18,19} largely because of improved ignition of lean mixtures. This results from the spark kernel exiting the igniter as a small jet, which increases the penetration of the plasma and hot gases and improves the turbulent mixing¹⁶. In pulsed plasma jet igniters the spark is generated in a cavity¹⁰. As the spark develops the temperature rises quickly, causing a sharp increase in the pressure within the cavity. The large pressure gradient causes a spherical shock wave to form at the cavity exit and the plasma is ejected as a supersonic jet. The plasma jet rapidly mixes with the surroundings and cools. Within approximately five microseconds, the temperature of the plasma drops sufficiently so it is no longer luminous¹⁶. As the jet of heated gases slows, it develops into a small turbulent element or “puff”. The kernel continues to mix with the surrounding air, causing the kernel temperatures to return to ambient values. A thorough discussion of the aerodynamics of spark kernels exiting from plasma jet igniters has been reported by Topham et al.¹⁶.

B. Radiation Intensity Measurements

Figure 1 illustrates the experimental arrangement used for acquiring the radiation intensity measurements. An infrared camera lens was positioned 29.5 cm away from the center of the igniter. At this distance the spatial resolution of each pixel was 0.16 mm² at the center of the igniter. A polished stainless steel mirror was placed behind the igniter to enable simultaneous visualization of top and side views of the spark kernels. Shields were placed on two sides of the igniter to minimize disturbances from the surrounding air. Sparks were generated at 45 Hz. The sampling frequency of the camera was set to 1260 Hz, although the actual sampling frequency varied due to limitations in transferring the data from the camera to the computer. Differences between the sampling and sparking frequencies allowed measurements to be acquired of kernels at various heights above the igniter.

Measurements were acquired with the detector integration time set to 0.03 and 0.4 ms. The former setting was used for quantitative measurements while the latter setting was used for qualitative visualization for reasons to be discussed. A heated plate was placed behind the igniter when an integration time of 0.03 ms was used (qualitative measurements) to ensure that the response of the focal plane array was linear for the measurements from the side. The intensity of the spark kernel was determined by subtracting the average measured intensity of the heated plates from the measurements with both the kernel and the heated plate. An integration time of 0.4 ms was used to increase the sensitivity of the camera. Kernel images farther above the igniter could be visualized with this setting than those acquired with an integration time of 0.03 ms, as a result of the increased sensitivity. Images acquired with the integration time of 0.4 ms are qualitative because of spatial blurring.

In the measurements where the kernel was observed exited the igniter the camera focal plane array was typically saturated by the radiation emitted from the kernel. It is plausible that the high levels of radiation are in part emitted from plasma in the flow. Reducing the integration time of the camera below 0.03 ms failed to eliminate detector saturation. Images where saturation of the detector occurred were not processed to avoid biasing the results.

The camera was calibrated using a blackbody source. Photon counts reported by the camera were correlated to the known radiation intensity emitted by the blackbody. The camera focal plane array responds linearly to increases in intensity. The intensity which could be detected above the camera noise is 0.1 W/m²-sr.

The camera measures the spectrally integrated radiation intensity,

$$I_{\Delta\lambda} = \int_{\lambda_1}^{\lambda_2} \alpha_{\lambda} I_{\lambda} d\lambda . \quad (1)$$

α_{λ} is the spectral absorption coefficient which accounts for variations in the spectral response of the camera, and losses through the camera optics. λ_1 and λ_2 are the spectral range of the camera, 3-5 μm . Within this spectral range the camera detects primarily radiation emitted by carbon dioxide (CO₂) and water vapor (H₂O) in the air. The subscript $\Delta\lambda$ is used to differentiate from the total intensity (I) which is obtained by integrating over all wavelengths. The spectral intensity (I_{λ}) emitted by the kernels can be described by solving the radiation transfer equation for a homogenous non-scattering medium²⁰,

$$I_{\lambda} = I_{\lambda}(0)e^{-\tau_{\lambda}} + \int_0^{\tau_{\lambda}^*} I_{b\lambda}(\tau_{\lambda}^*)e^{-(\tau_{\lambda}-\tau_{\lambda}^*)} d\tau_{\lambda}^* , \quad (2)$$

where τ_{λ} is the optical thickness defined as,

$$\tau_{\lambda} = \int_0^s \kappa_{\lambda} ds . \quad (3)$$

κ_{λ} is the linear absorption coefficient and s is the path length through the radiating medium. $I_{b\lambda}$ is the blackbody spectral intensity described by the Planck distribution²¹.

B. Temperature and Delivered Energy Values

An inverse deconvolution technique was implemented to estimate the temperature and sensible energy of the kernels. Similar approaches have been used to estimate water vapor concentrations in a hydrogen flame, determine integral time and length scales in turbulent flames, and scalar concentrations in a pool fire²²⁻²⁴.

The kernel was divided into a series of disks with a known diameter (d), as illustrated in Figure 2. The edge of the kernel was defined as the location where the intensity equaled twice the noise level of the detector (0.2 W/m²-sr). Geometric relationships were used to determine the corresponding path lengths (s_i) through the kernel. Carbon dioxide and water vapor concentrations were assumed to be atmospheric values. The following procedure was implemented to estimate the temperature within the kernels using the path lengths and species concentrations:

- 1) A temperature was guessed for a line of sight path through the kernel.
- 2) The spectral intensity was calculated by solving the radiation transfer equation (Eq. (2)) using a narrowband radiation model (RADCAL²⁵). The path length, guessed temperature, and atmospheric carbon dioxide and water vapor mole fractions were inputs to the model.
- 3) The spectral intensity was multiplied by the absorption coefficient and spectrally integrated ((Eq. (1)) to determine the intensity.
- 4) The calculated and measured intensity were compared, the guessed temperature was updated, and steps (1) – (3) were repeated until the intensity values converged.
- 5) Temperatures for neighboring lines of sight were calculated using steps (1) – (4) for all radial locations at that height above the igniter.
- 6) Steps (1) – (5) were repeated at each height until values were found for the entire domain.

This approach provides path integrated temperature values. Infrared images indicate that the spark develops into a ring with high radiation intensity toward the outer edges. Theoretically the thickness of the ring could be estimated from the top view of the kernels and used in conjunction with the spatial deconvolution. The high radiation intensity being emitted by the igniter, however, limited the ability to accurately determine the ring thickness. The sensitivity of the deconvoluted temperature to changes in the path length, such as developing into rings, is reported in the next section.

The sensible energy of the kernel (U) was estimated by summing the sensible energy along each line of sight (i),

$$U = \sum_{i=1}^N s_i h_i w_i \frac{P}{RT_i} C_v (T_i - T_\infty) . \quad (4)$$

h_i and w_i are the height of each disk and the distance between lines of sight respectively. The sensible energy of the kernels reduces downstream due to mixing with the surrounding air. The total sensible energy of the spark and that transferred to the surroundings (which is conserved) is not captured in the measurements due to the detection limits of the camera.

Over 600 kernel images were acquired and used for determining the average temperature, sensible energy, and trajectory. Only values at axial and radial locations where radiation from the kernel was detected at least 30 times are reported to allow for a sufficient sample size. Atmospheric values are reported at the other locations. Average values are reported 0.75 cm above the igniter and beyond. Between the igniter exit and 0.75 cm downstream, saturation of the camera focal plane array was observed in some of the images. Images where saturation of the detector occurred were neglected to avoid biasing the results. The average sensible energy of the sparks is reported at 0.25 cm increments downstream of the igniter. The value at each axial location is the average sensible energy of the sparks whose centers are within a 0.25 cm region.

C. Evaluation of Technique

The average percent change in the deconvoluted temperature and sensible energy due to variations in the deconvolution parameters are reported in Figures 3 and 4 respectfully. Changes in the measured intensity, path length through the kernel, and carbon dioxide and water vapor mole fractions were assessed for two kernel images. The average temperature changes by less than 25% for up to a 60% variation in the measured intensity and radiating species mole fractions. Changes in the temperature due to variations in the path length are similar to changes in the carbon dioxide mole fraction (less than 20% error) for a -40% to 60% change in the deconvolution parameter. A 60% reduction in the path lengths through the kernels results in a 90% increase in the temperature. The sensible energy changes by less than 20% for up to a 60% variation in the measured intensity and radiating species mole fractions. The sensible energy is less susceptible to changes in the intensity and radiation species concentrations because of the inverse dependence of sensible energy on the kernel temperature (Eq. 4). The average sensible energy changes by less than 65% for a 60% error in the path lengths. It is noted that the percent change in the sensible energy is opposite in sign than the percent change in temperature for equivalence changes in path lengths. This results from the linear dependence of sensible energy on the path length and inverse dependence on kernel temperature.

The deconvolution technique was used to determine the temperature of a partially premixed hydrogen flame anchored to a Hencken burner. This flame has been well characterized by CARS measurements^{26,27}. A temperature profile²⁶ was assumed toward the edges of the flame in the deconvolution technique. Figure 5 reports the comparison between the CARS and deconvoluted peak temperature values. The deconvoluted temperatures agree with measured values^{26,27} within 15%. The deconvolution approach captures the increase in temperature for an increase in equivalence ratio. For all equivalence ratios the deconvoluted temperatures are underestimated. It is suspected that is caused by differences between the physical and modeled spectral absorption, and uncertainties in the radiation intensity measurements and narrowband radiation model.

The time resolved deconvoluted temperature values reported in this work are normalized by a representative temperature (near igniter exit) found using backward oriented schlieren (T_{BOS}). This allowed for further evaluation of the deconvolution technique. The backward oriented schlieren temperatures were found for kernels exiting from the same igniter into quiescent air.

III. Results and Discussion

A. Infrared Images

Simultaneous top and side view images of spark kernels are shown in Fig. 6. Images were taken using an integration time of 0.4 ms to allow for qualitative visualization. The time between consecutive images is approximately 0.8 ms. The brightest colors are the regions of highest radiation intensity. The first image in Fig. 6 is of a kernel just after exiting the igniter. By the second image the kernel transitions into a high intensity ring shape, as evident from the top view. The formation of the kernel into a ring has been noted for typical spark systems¹⁴ (i.e. without a cavity) and for pulsed plasma torches²⁸. The development of the kernels into rings when exiting from this igniter is noteworthy considering that some models¹⁶ have assumed the kernel is spherical. It is theorized that a

toroidal vortex forms as the heated gas and plasma eject from the igniter cavity. The vortex entrains fluid into the center of the kernel which decreases the temperature and subsequently the radiation intensity.

Side view images of the kernel show a region with higher intensity followed by a tail with lower intensity. These are similar to shadowgraph images reported by Borghese et al.²⁹. The size of the kernel in the infrared images decays downstream as the kernel mixes with the surrounding air.

Images were taken with the igniter positioned parallel to the horizon with the camera facing the igniter cavity to assess the importance of buoyancy forces. The spark kernels did not consistently rise with respect to the horizon, as would be expected if buoyancy forces were significant. This indicates that kernels exiting from this type of igniter are momentum dominated within the time span (order of ms) that images were acquired. This is in agreement with the work reported by Topham et al.¹⁶.

C. Time Resolved Values

Time resolved radiation intensity measurements of three representative sparks are reported in Fig. 7. The detector integration time was set to 0.03 ms to eliminate spatial blurring and provide quantitative values. Measurements of the kernel just above and downstream of the igniter are superposed for comparison. In the vicinity of the igniter (e.g. $z = 0.75$ cm) the kernels are nearly spherical in shape from the side view. The kernel diameters are greater than 1 cm based on the infrared images. Peak intensity values between 7 and 10 W/m²-sr are observed, at least an order of magnitude smaller than the intensity emitted by the kernels as they exit the igniter. Recall that the camera focal plane array is typically saturated (at 285 W/m²-sr) in the images where the kernels exit the igniter. The intensity observed in Fig. 7 varies spatially within the kernels indicating temperature variations. The small regions of high intensity observed both in and outside of the kernels are radiation emitted by material ablating off from the igniter. The deconvoluted temperature values which were above 2400 K in these regions were neglected when averaging.

The size of the kernels and the radiation intensity emitted by them decays rapidly downstream of the igniter. Between 2 and 2.5 cm downstream the peak intensity in the images reduces by approximately a factor of 3 to values between 2 and 3 W/m²-sr. Regions of higher and lower radiation intensity remain evident. Both the radius and height of the kernel reduce such that the kernel becomes approximately oval in shape. Mixing of the kernel with the surrounding air causes the reduction in size.

Figure 8 presents the path integrated temperatures values corresponding to the intensity measurements reported in Fig. 7. Values are normalized with respect to a typical value obtained using backward oriented schlieren. Between 0.5 and 1.5 cm downstream the kernel temperatures are nearly within 30% of the backward oriented schlieren value. Peak temperature values generally occur in the regions where the highest radiation intensity is observed, as would be expected. In some instances higher temperatures are observed toward the edges of the kernels. This is an artifact of determining the path lengths through the kernel by dividing the domain into a series of disks. Path lengths are shorter at the edges of the disk, resulting in higher temperatures for equivalent intensity values.

D. Mean Values

The average radiation intensity of the spark kernels between 0.75 and 3.25 cm above the igniter is reported in Fig. 9. The peak average intensities decay from near 3.5, to 1.5 W/m²-sr between 1 and 2 cm above the igniter. At 3 cm above the igniter the average intensity is negligible. Near 1.5 cm above the igniter, the centerline intensity is lower than radial locations in the immediate vicinity (e.g. $r = \pm 0.3$ cm). This is attributed to the ring shape of the kernel. Peak radiation intensity values occur toward the edges of the high temperature gaseous rings; the path length through the medium is the longest in this region. This is the reason that higher intensities have been observed off the flame centerline of a laminar diffusion flame²². In this flame a ring of hot exhaust products surrounds the cooler fuel jet.

Figure 10 presents the statistical distribution of the kernel trajectories. The number of times radiation from a kernel was detected (above the camera noise) at a location is normalized by the total number of kernel images. Kernels were detected approximately 70% of the time between 0.75 and 1.25 cm above the igniter and for radii within 0.3 cm of the centerline. Above this region, kernels were observed less frequently. At 2 cm above the igniter and beyond, kernels were detected less than 30% of the time. This reduction occurs primarily because the kernels decrease in size downstream in the infrared images. Kernels were detected at radial locations 0.75 cm away from the centerline 10% of the time (e.g. $z = 1.5$ cm). This indicates that the trajectory of a fraction of the kernels is away from the centerline.

The normalized average spark kernel temperatures are reported in Fig. 11. Values are found from the time resolved images, and are normalized by the peak temperature at 0.75 cm downstream to illustrate the decay in the temperature. The average temperature decays by less than 30% at nearly all locations where radiation from the spark

is detected. The relative reduction in temperature is smaller than the reduction in the intensity values (Fig. 9) due to the nonlinear dependence of radiation intensity on the temperature. It is noted that the highest normalized temperatures occur near radial locations corresponding to 0.5 cm away from the centerline. This results from the path averaging nature of the approach. The temperature in the center of the rings is cooler than toward the outer edges.

Figure 12 presents the normalized average sensible energy of the kernels. The energy decays in a linear manner ($R^2=0.98$). Between 0.75 and 2.5 cm above the igniter, 80% of the sensible kernel energy is dissipated to the surroundings based on the detected radiation intensity. This results from mixing of the kernel with the surrounding air.

IV. Summary and Conclusions

In this work the radiation intensity emitted from spark kernels exiting from a pulsed plasma jet igniter was measured using an infrared camera. The trajectory and spatial development of the kernels were assessed from the images. An inverse deconvolution technique was developed to determine path integrated temperature values. The deconvolution technique was evaluated using a sensitivity analysis and comparisons to measurements of a well characterized flame. Sensible energy values are reported at varying axial locations based on the deconvoluted temperatures.

The specific conclusions of this work are as follows:

- 1) Spark kernels exiting from pulsed plasma jet igniters develop into a toroidal shape downstream of the igniter.
- 2) The trajectory of kernels varies between spark events. The statistical distribution of the spark trajectory is symmetric when exiting into quiescent air.
- 3) The radiation intensity emitted by spark kernels decreases by more than an order of magnitude after exiting the igniter. Variations in the intensity within a kernel indicate temperature variations.
- 4) Temperature values decreased by less than 30% within the region that radiation from kernels was detected.
- 5) The sensible energy of the kernels decays in a linear manner. In less than 2 cm the sensible energy decayed by 80%.

Acknowledgments

This project was performed while the corresponding author was performing a Summer Research Fellowship at the Combustion Branch of Air Force Research Laboratories. Funding from AFRL supported the continuation of this work. Sukesh Roy provided technical mentoring. Paul Litke, Steve Bolton, and Amy Lynch aided in developing the experimental arrangement and acquiring data. Larry Goss provided backward oriented schlieren temperature values. Daniel Richardson helped with acquiring the radiation intensity measurements of the Hencken burner flames. Jay Gore is the academic advisor for the corresponding author. His tutelage is gratefully acknowledged.

References

- ¹Ekcici, O., Ezekoye, O., Hall, M., Mathews, R., "Thermal and Flow Fields Modeling of Fast Spark Discharges in Air," *Journal of Fluids Engineering*, Vol. 129, No. 11, 2007, pp. 55-65.
- ²Song, J., Sunwoo, M., "Analysis of Flame Kernel Development with Schlieren and Laser Deflection in a Constant Volume Combustion Chamber," *Proceedings of the Institution of Mechanical Engineers, Part D: Journal of Automobile Engineering*, Vol. 216, 2002, pp. 581-590.
- ³Arpacı, V., Ko, Y., Lim, M., Lee, H., "Spark Kernel Development in Constant Volume Combustion," *Combustion and Flame*, Vol. 135, 2003, pp. 315-322.
- ⁴Dale, J., Checkel, M., Smy, P., "Application of High Energy Ignition Systems to Engines," *Progress in Energy and Combustion Science*, Vol. 23, 1997, pp. 379-398.
- ⁵Naegeli, D., Dodge, Lee, "Ignition Study in a Gas Turbine Combustor," *Combustion Science and Technology*, Vol. 80, 1991, pp. 165-184.
- ⁶Au, S., Haley, R., Smy, P., "The Influence of the Igniter-Induced Blast Wave Upon the Initial Volume and Expansion of the Flame Kernel," *Combustion and Flame*, Vol. 88, 1992, pp. 50-60.
- ⁷Hillard, J., Springer, G. eds., Maly, R. athr., *Fuel Economy: in Road Vehicles Powered by Spark Ignition Engines*, 1984, Chapter 3.
- ⁸Heywood, J., *Internal Combustion Engine Fundamentals*, McGraw-Hill, New York, 1988, p. 429.
- ⁹Reinmann, R., Akram, M., "Temporal Investigation of a Fast Spark Discharge in Chemically Inert Gas," *Journal of Physics D: Applied Physics*, Vol. 30, 1997, pp. 1125-1134.
- ¹⁰Carleton, F., Vince, I., Weinberg, F., "Energy and Radical Losses from Plasma Jet Igniters to Solid Surfaces," *Nineteenth Symposium (International) on Combustion*, Vol. 19, 1982, pp. 1523-1531.

- ¹¹Smy, P., Clements, R., Dale, J., Simeoni, D., Topham, D., "Efficiency and Erosion Characteristics of Plasma jet Igniters," *Journal of Applied Physics D: Applied Physics*, Vol. 16, 1983, pp. 783-791.
- ¹²Ko, Y., Anderson, R., Arpaci, V., "Spark Ignition of Propane-Air Mixtures Near the Minimum Ignition Energy: Part I. An Experimental Study," *Combustion and Flame*, Vol. 83, 1991, pp. 75-87.
- ¹³Zhang, J., Clements, R., Smy, P., "An Experimental Investigation of the Effect of a Plasma Jet on a Freely Expanding Methane-Air Flame," *Combustion and Flame*, Vol. 50, 1983, pp. 99-106.
- ¹⁴Borghese, A., Diana, M., Moccia, V., Tamai, R., "Early Growth of Flames, Ignited by Fast Sparks," *Combustion Science and Technology*, Vol 76, 1991, pp. 219-231.
- ¹⁵Borghese, A., D'alessio, A., Diana, M., Venitozzi, C., "Development of Hot Nitrogen Kernel, Produced by a Very Fast Spark Discharge," *Twenty-Second Symposium (International) on Combustion*, Vol. 22, 1988, pp. 1651-1659.
- ¹⁶Topham, D., Clements, R., Smy, P., "Turbulent Mixing in a Pulsed Plasma jet Exhaust," *Journal of Fluid Mechanics*, Vol. 148, 1984, pp. 207-224.
- ¹⁷Kono, M., Niu, K., Tsukamoto, T., Ujiie, Y., "Mechanism of Flame Kernel Formation Produced by Short Duration Sparks," *Twenty-Second Symposium (International) on Combustion*, Vol. 22, 1988, pp. 1643-1649.
- ¹⁸Low, C., Wilson, C., Abdel-Gayed, R., Bradley, D., "Evaluation of Novel Igniters in a Turbulent Bomb Facility and a Turbo-Annular Gas Turbine Combustor," *AIAA 25th Joint Propulsion Conference*, Monterey, CA, 1989-2944.
- ¹⁹Gardiner, D., Mallory, R., Pucher, G., Todesco, Marc, Bardon, M., Batista, V., "Experimental Studies Aimed at Lowering the Electrical Energy Requirements of a Plasma jet Ignition System for M100 Fuelled Engines," *SAE Technical Paper Series*, 1996, paper. 961989.
- ²⁰Siegel, R., Howell, J., *Thermal Radiation Heat Transfer*, 3rd ed., Hemisphere Publishing Corporation, Washington, 1992, p. 688.
- ²¹Modest, M., *Radiative Heat Transfer*, 2nd ed., Academic Press, San Diego, 2003, p. 267.
- ²²Blunck, D., Basu, S., Zheng, Y., Gore, J., "Simultaneous Water Vapor Concentration and Temperature Measurements in Unsteady Hydrogen Flames," *Proceedings of the Combustion Institute*, Vol. 32, 2009, 2527-2534.
- ²³Zheng, Y., Barlow, R., Gore, J., "Spectral Radiation Properties of Partially Premixed Turbulent Flames," *Journal of Heat Transfer*, Vol. 125, 2003, pp. 1065-1073.
- ²⁴Biswas, K., Zheng, U., Kim, C., Gore, J., "Stochastic Time Series Analysis of Pulsating Buoyant Pool Fires," *Proceedings of the Combustion Institute*, Vol. 31, 2007, pp. 2581-2588.
- ²⁵Grosshandler, W., Technical Note TN1402, National Institute of Science and Technology, 1993.
- ²⁶Hancock, R., Bertagnolli, K., Lucht, R., "Nitrogen and Hydrogen CARS Temperature Measurements in a Hydrogen/Air Flames Using a Near-Adiabatic Flat-Flame Burner," *Combustion and Flame*, Vol. 109, 1997, pp. 323-331.
- ²⁷Roy, S., Kinnius, P., Lucht, R., Gord, J., "Temperature Measurements in Reacting Flows by Time-Resolved Femtosecond Coherent anti-Stokes Raman Scattering (fs-CARS) Spectroscopy," *Optics Communication*, Vol. 281, 2008, pp. 319-325.
- ²⁸Merica-Bourdet, N., Laroussi, M., Begum A., Karakas, E., "Experimental Investigations of Plasma Bullets," *Journal of Physics D: Applied Physics*, Vol. 42, 2009, pp. 1-7.
- ²⁹Borghese, A., Diana, M., Moccia, V., Tamai, R., "Enhancing Ignition by Conditioning the Fast-Spark Induced Flow Field," *International Symposium on Diagnostics and Modelling of Combustion in Reciprocating engines*, 1990, pp. 159-165.

Figures:

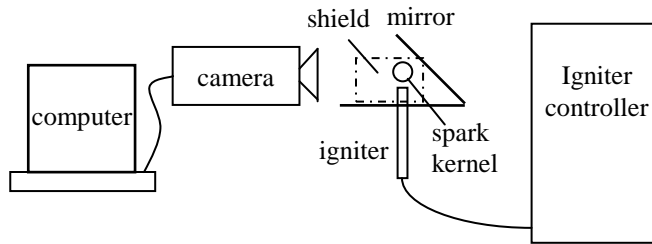


Figure 1. Experimental arrangement for obtaining radiation intensity measurements of spark kernels.

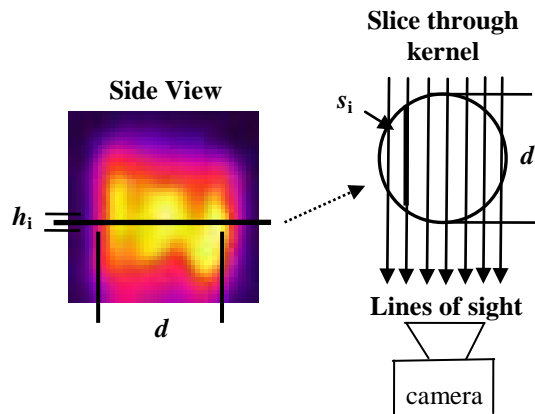


Figure 2. Schematic of deconvolution approach used for inverse calculations.

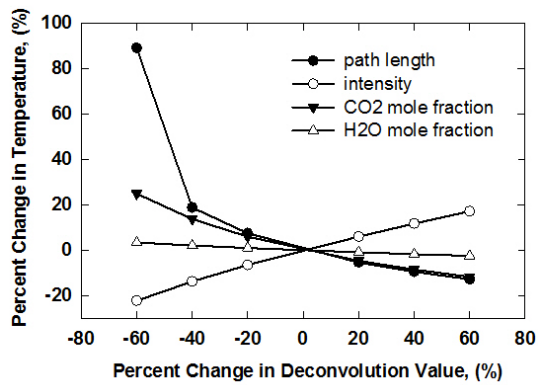


Figure 3. Percent change in the average deconvoluted temperature with respect to changes in deconvolution parameters.

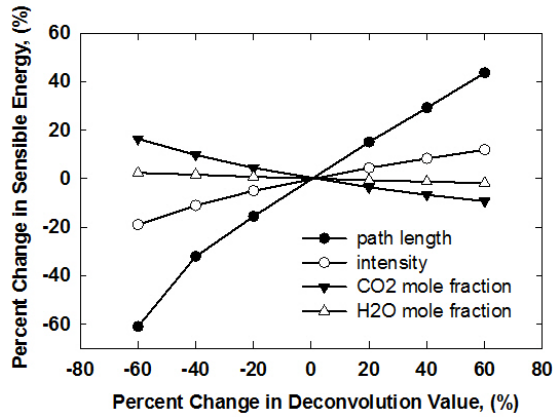


Figure 4. Percent change in the average deconvoluted sensible energy with respect to changes in deconvolution parameters.

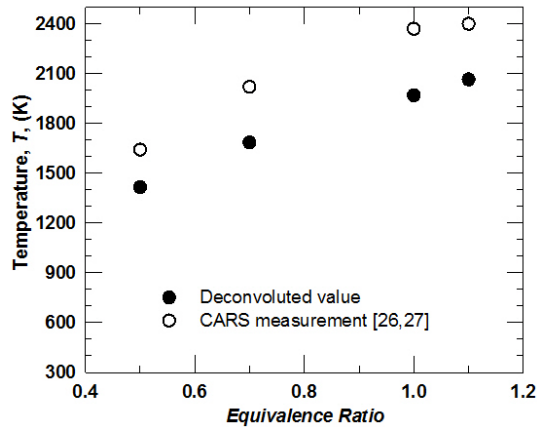


Figure 5. Deconvoluted and measured temperature values of partially premixed hydrogen flames anchored to a Hencken burner.

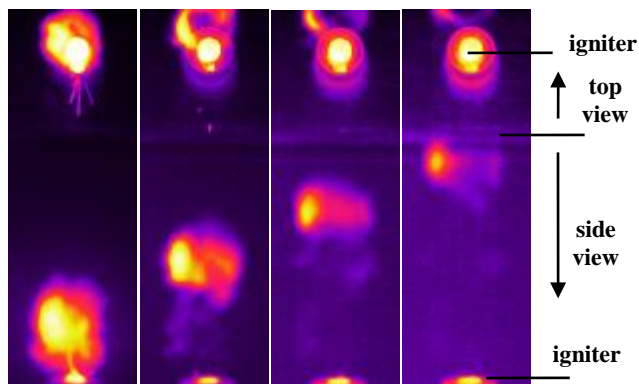


Figure 6. Simultaneous infrared images of top and side views a spark kernel at varying heights above the igniter. The time between the images is 0.8 ms.

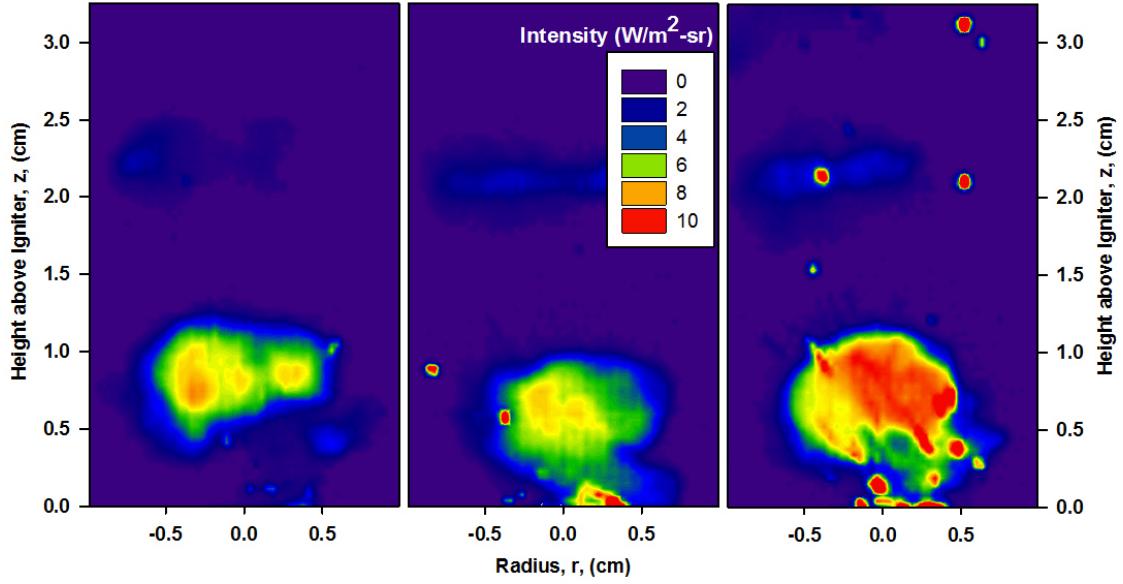


Figure 7. Time resolved radiation intensity measurements of spark kernels.

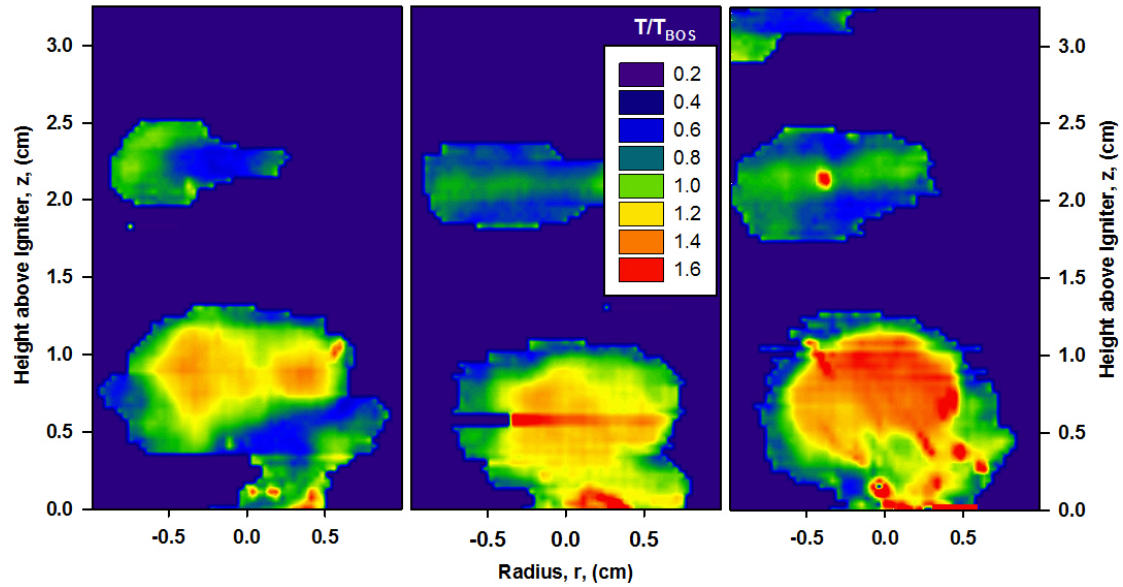


Figure 8. Time resolved deconvoluted temperature values of spark kernels normalized by a typical value obtained using backward oriented schlieren (T_{BOS}).

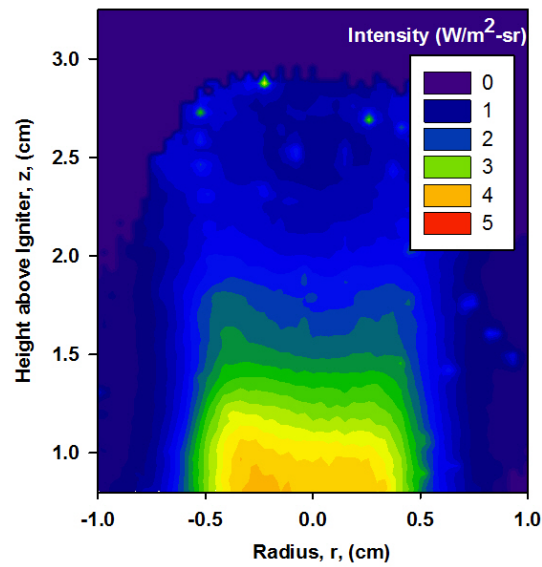


Figure 9. Mean radiation intensity emitted from spark kernels.

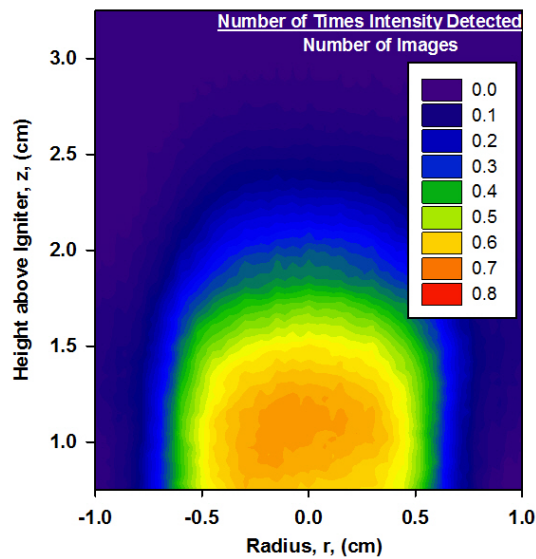


Figure 10. Spatial distribution of spark kernel trajectories. The number of times radiation from a kernel is detected at a location is normalized by the number of kernel images.

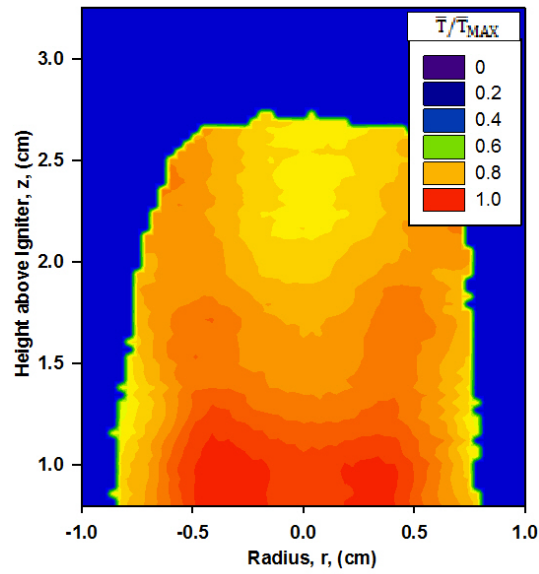


Figure 11. Normalized average temperature of spark kernels.

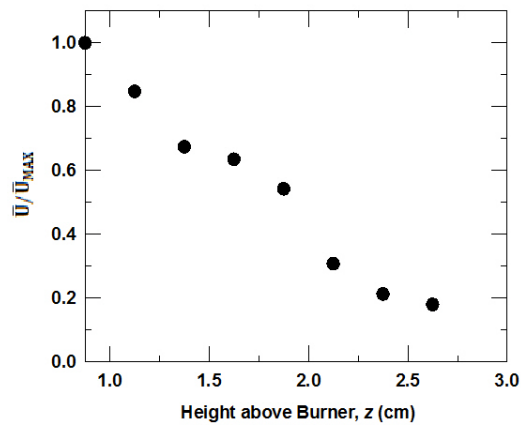


Figure 12. Average sensible energy of spark kernels normalized by the average value near 0.9 cm above the burner.